Research paper

Active photocatalytic water splitting solar-to-hydrogen energy conversion: Chalcogenide photocatalyst Ba$_2$ZnSe$_3$ under visible irradiation

A.H. Reshak

New Technologies − Research Centre, University of West Bohemia, Univerzitni 8, 306 14, Pilsen, Czech Republic

ABSTRACT

The photocatalytic performance of Ba$_2$ZnSe$_3$ is investigated by means of density functional theory. The investigation confirms that Ba$_2$ZnSe$_3$ possesses large birefringence, considerable anisotropy in the optical response, and the absorption edge occurs in the visible region. The estimated optical band gap of Ba$_2$ZnSe$_3$ is about 2.70 eV, and the EPc and EPv are about -0.145 V(vs.NHE) and $+2.605$ V (vs.NHE), respectively. Thus, Ba$_2$ZnSe$_3$ possesses a high negative reduction potential of excited electrons due to its higher CB position, and hence, the location of the CBM and VBM accommodates the redox capacity. Thus, the Ba$_2$ZnSe$_3$ photocatalyst is expected to exhibit superior activity in visible-light-driven photocatalytic H$_2$ evolution. The electronic band structure shows high k-dispersion bands around the Fermi level, which implies low effective masses and, hence, the high mobility carriers enhance the charge transfer process. It was found that Ba$_2$ZnSe$_3$ possesses a great effective mass difference between electron (e^-) and hole (h^+), which can facilitate the e^- and h^+ migration and separation, and finally improve the photocatalytic performance. The observed large mobility difference in Ba$_2$ZnSe$_3$ is useful to the separation of e^- and h^+, reduction of the e^- and h^+ recombination rate, and improvement of the photocatalytic activity. Thus, Ba$_2$ZnSe$_3$ could be a good photocatalyst due to rapid generation of $e^- - h^+$ pairs with photoexcitation, and a high negative reduction potential of excited electrons due to its higher CB position. The excellent photocatalytic performance of Ba$_2$ZnSe$_3$ is due to hyperpolarizablity formed by ZnO$_4$ tetrahedra and co-parallel BaSe$_7$ polyhedra groups, and the layer structure favors the enhancement of the photocatalytic performance. The presence of the distorted $(ZnO_4)^{4-}$ tetrahedral causes to increase the efficiency of the photocatalytic performance almost to double in comparison to other chalcogenide crystals. Based on these results, one can conclude that Ba$_2$ZnSe$_3$ satisfies all requirements to be an efficient photocatalyst. This will greatly improve the search efficiency and greatly help experiments to save resources in the exploration of new photocatalysts with good photocatalytic performance.

1. Introduction

The search for novel photocatalysts, materials with promising structural and photocatalytic performance, is still a challenge for scientists. To produce efficient photocatalytic performance, the materials should possess high mobility carriers, suitable band gap width and, hence, higher absorption capacity [1,2]. Therefore, a balance between the light absorption capacity and the reduction power in the investigated material leads to a higher efficiency of light-driven photocatalytic H$_2$ production [3,4]. The other important requirement is, the photocatalysts must show efficient separation and migration ability of the photoexcited carriers, due to the fact that the photocatalytic reaction utilizes the photoexcited electrons (e^-) and holes (h^+) migrating to the surface of the photocatalyst. The photocatalysis process does not produce any pollutants because it uses photon energy and water, and hence, it will make a great contribution to energy and environmental

challenges in the near future. Also, the high-performance photocatalyst system requires low recombination of photogenerated e^- and h^+ to ensure that the reduction and oxidation reactions can occur favorably in the conduction band (CB) and valence band (VB) of a semiconductor photocatalyst [5]. However, it remains challenging to efficiently design a suitable high-performing photocatalyst material.

Photocatalytic water splitting is one of the most promising strategies to achieve clean and renewable solar-to-hydrogen energy conversion [6–26]. The development of visible-light-responsive photocatalysts has been attracting several researchers in recent years [13–27]. Among the various types of visible-light-responsive photocatalysts, Ba$_2$ZnSe$_3$ could be considered because of its optical gap (2.7 eV, λ = 459.1 nm), well matched with the solar spectrum, and the sufficient negative conduction band potential for reduction of H$^+$/H$_2$ [28–30]. TiO$_2$ is one of the traditional photocatalysts which possess a wide energy band gap that makes this photocatalyst active in the ultraviolet region only. This

implies that TiO_2 utilizes only 3–5% of the sunlight. Thus, tremendous research work has been carried out to exploit the solar radiation more efficiently [31–33]. Among the promising candidates are the chalcogenides, which are a large family with complex structure, appropriate chemical and physical properties, and relatively small energy band gaps. This makes them promising candidates for visible-light harvesting [34–36].

Zn-based chalcogenides are expected to be superior photocatalysts due to their small energy band gaps and huge photosensitivity [37–43]. Recently Zhou et al. [44] synthesized a novel promising visible-light chalcogenide photocatalyst, Ba_2ZnSe_3, by traditional solid-state reaction. The thermal and optical properties of Ba_2ZnSe_3 were investigated and it was found to be thermally stable and it does not undergo phase transition from 106 K to room temperature. Furthermore, Zhou et al. preformed photocatalytic H_2-production experiments which proved that Ba_2ZnSe_3 is a versatile material for photocatalytic H_2 evolution. The photocatalytic activity experiment, photo-electrochemical test, and thermal measurement indicate that Ba_2ZnSe_3 shows good visible-light-responsive photocatalytic efficiency and excellent thermal stability and cyclability, which are favorable for its application. This feature makes Ba_2ZnSe_3 a promising candidate as an active photocatalyst [44]. For detailed information regarding the photocatalytic H_2-production experiments, we refer readers to Ref. 44. Prakash et al. [45] synthesized two new ternary chalcogenides Ba_2ZnQ_3 (Q = Se, Te) and investigated their crystal structure, and optical and electronic properties.

As a natural extension to the work of Zhou et al. [44] and Prakash et al. [45], we addressed ourselves to further comprehensive investigation to support the Zhou et al. finding that Ba_2ZnSe_3 is a promising photocatalyst. In this work, *ab-inito* calculations from first- to second-principles methods are performed to investigate the suitability of Ba_2ZnSe_3 to be used as an active photocatalyst under visible light irradiation.

2. Methodology

The chalcogenide Ba_2ZnSe_3 crystallizes in orthorhombic symmetry with space '*Pnma*' (No. 62). The experimental lattice parameters are a = 9.0744 (2) Å, b = 4.4229 (1) Å, c = 17.6308 (4) Å and Z = 4 [44]. As the first step, a geometrical relaxation was performed for the experimental x-ray diffraction of chalcogenide Ba_2ZnSe_3 [44] using the Perdew-Burke-Ernzerhof generalized gradient approximation (PBE − GGA) [46]. The resulting relaxed geometry in comparison with the experimental data [44] is provided as a supplementary material. A good agreement was found between the relaxed geometry and the experimental data. The relaxed geometry is shown in Fig. 1. One can see that each Zn atom is coordinated with four Se atoms, forming a $ZnSe_4$ distorted tetrahedron; the Zn atom is linked to the four Se atoms with different bond lengths. The resulting $ZnSe_4$ distorted tetrahedron shares two corners with its neighbor to form infinite chains of $[ZnSe_4]^{4-}$ units (see Fig. 1b). These $[ZnSe_4]^{4-}$ units are separated by Ba atoms, where each Ba atom is surrounded by seven Se atoms in a monocapped trigonal prismatic geometry to form $BaSe_7$ polyhedra (see Fig. 1c,d).

Using the obtained relaxed geometry, the ground state and photocatalytic properties are calculated using the all-electrons full-potential linear augmented plane wave (FPLAPW + lo) method as embodied in the Wien2k code [47], utilizing the modified Becke-Johnson potential (mBJ) to treat the exchange correlation [48]. The mBJ is a local approximation of an atomic "exact-exchange" potential and a screening term which allows the calculation of band gaps with accuracy similar to the very expensive GW calculations [48]. The muffin-tin radii (R_{MT}) of Ba, Zn and Se atoms were chosen in such a way that the spheres did not overlap. The value of R_{MT} is taken to be 2.5 a.u. (Ba), 2.25 a.u. Zn), and 2.14 a.u. (Se). To achieve the total energy convergence, the basis functions in the interstitial region were expanded up to $R_{MT} \times K_{max}$ = 7.0. The maximum value of l was taken as l_{max} = 10, while the charge density is Fourier expanded up to G_{max} = 12 $(a.u)^{-1}$.

Self-consistency is obtained using 1500 $\vec{k}$ points in the irreducible Brillouin zone (IBZ). The self-consistent calculations are converged when the total energy of the system is stable within 0.00001 Ry. The calculations of the electronic band structure, density of states and electronic charge density distribution are performed with 5000 $\vec{k}$ points in the IBZ. In this study we provide a detailed investigation concerning the suitability of chalcogenide Ba_2ZnSe_3 to be used as an efficient photocatalyst under visible light irradiation utilizing the first-principle material approaches.

In this work, *ab-inito* calculations from first- to second-principles methods are performed to investigate the suitability of chalcogenide Ba_2ZnSe_3 to be used as an active photocatalyst in the visible light region. It is well known that the DFT approaches have the ability to accurately predict the ground state properties of the materials, and the developed analytic tools are vital to investigating their intrinsic mechanism. This microscopic understanding has further guided molecular engineering design for new materials with novel structures and properties. It is anticipated that first-principle material approaches will greatly improve the search efficiency and greatly help experiments to save resources in the exploration of new crystals with good performance [49,50]. For instance, several researchers have used the first-principles calculation to explore new photocatalysts and found good agreement with the experimental results [51–57]. We would like to mention that, in our previous work [56–60], we have calculated the energy band gaps and the photophysical properties using the full-potential method for several systems whose energy band gaps and photophysical properties are known experimentally and a very good agreement with the experimental data was obtained. Thus, we believe that our calculations reported in this paper will produce very accurate and reliable results which will greatly help experiments to save resources in the exploration of new photocatalysts with good photocatalytic performance. The aim of this work is to focus on the photocatalytic activity of chalcogenide Ba_2ZnSe_3 as new, green and efficient photocatalyst.

3. Results and discussion

3.1. Structure-property relationship

It is well known that the photocatalytic activities are directly related to the materials' electronic structure [61]; therefore, the electronic band structure of chalcogenide Ba_2ZnSe_3 along the high symmetry directions of the first BZ is calculated to explore the bandś dispersion and the nature of the fundamental energy band gap, as shown in Fig. 2a. We set the zero-point of energy (Fermi level, E_F) at the valence band maximum (VBM). The VBM and conduction band minimum (CBM) are situated at Γ points of the BZ, resulting in a direct energy band gap of about 2.7 eV, in close agreement with the experimentally measured gap (2.75 eV) [44]. Therefore, the electrons (e^-) recombine directly with holes (h^+), which can increase the probabilities for photogenerated e^- and h^+ to participate in photocatalytic reactions. Moreover, the higher surface area-to-volume ratio allows for greater photon absorption on the photocatalyst surface, and increases the recombination of the $e^- - h^+$ pair. Therefore, the chalcogenide Ba_2ZnSe_3 is expected to show high photocatalytic activity. The schematic diagram of charge transfer and the photocatalytic mechanism of Ba_2ZnSe_3 are shown in Fig. 2b. The reactive species induced by illumination are responsible for the photodegradation process. If the energy of the incident photons is larger than the energy band gap of a photocatalyst, the e^- will be excited and transfer to the CBs, leaving h^+ in the VBs. Then the e^- have a great possibility to react with adsorbed oxygen to form another reactive species (superoxide $\cdot O_2^-$). In the meantime, the h^+ can also react with OH^- to generate hydroxyl ($\cdot OH$). The above-generated active species can all participate in the photocatalytic process.

To explore the type of orbitals which form the CBM and the VBM,
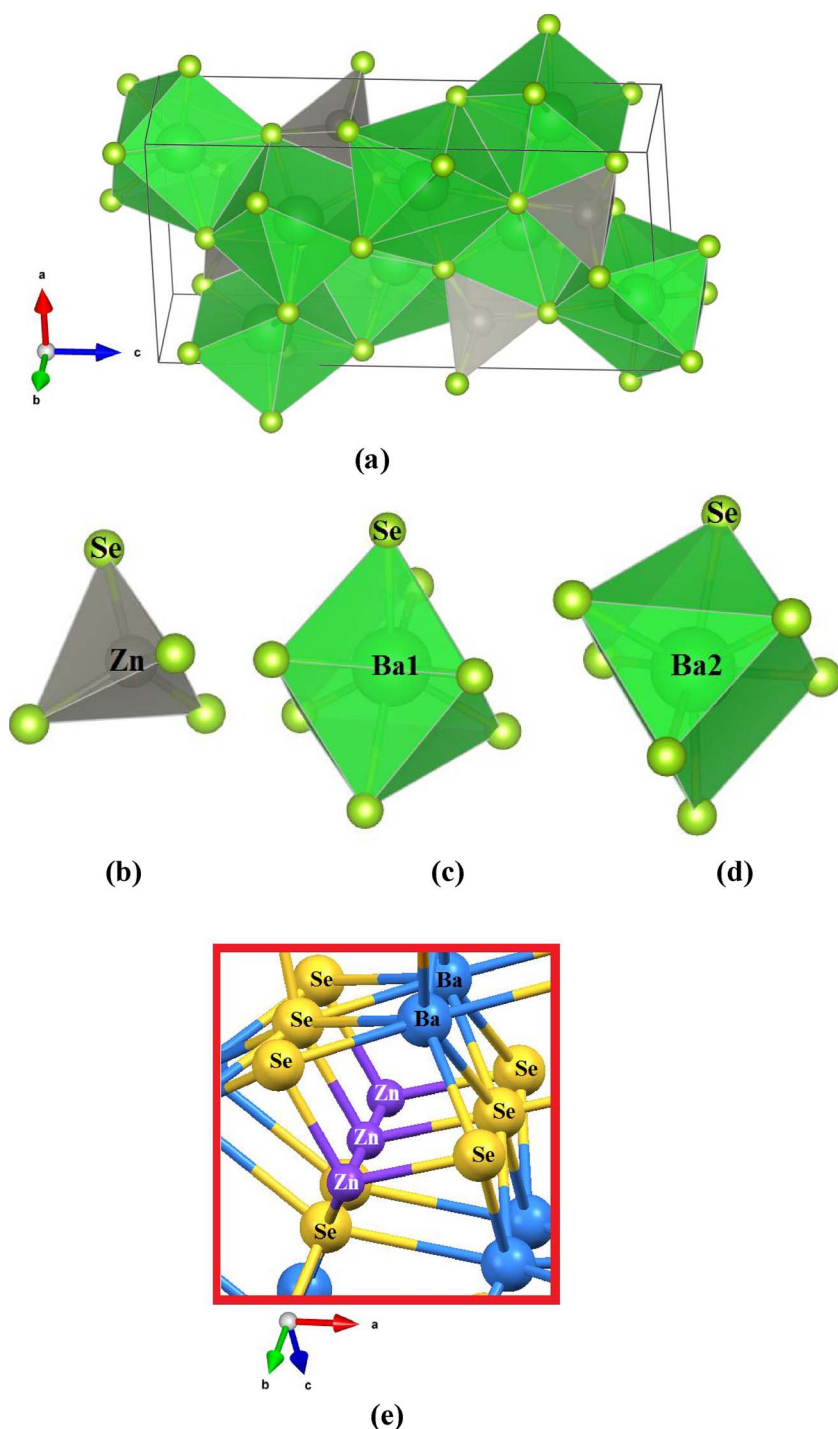
Fig 1. Crystal structure of chalcogenide Ba_2ZnSe_3. One can see that each Zn atom is coordinated with four Se atoms, forming a $ZnSe_4$ distorted tetrahedron; the Zn atom is linked to the four Se atoms with different bond lengths. The resulting $ZnSe_4$ distorted tetrahedron shares two corners with its neighbor to form infinite chains of $[ZnSe_4]^{4-}$ units (see Fig. 1a-e). These $[ZnSe_4]^{4-}$ units are separated by Ba atoms, where each Ba atom is surrounded by seven Se atoms in a monocapped trigonal prismatic geometry to form $BaSe_7$ polyhedra (see Fig. 1c,d).

the total and partial densities of states are investigated as shown in Fig. 2c–f. These figures reveal that the VBM is mainly formed by Se-p states with a small contribution from Ba-d and Zn-s/p states, whereas the CBM is formed by the Ba-d states with a small contribution from Zn-s/p states. This implies that the electron transition between VBM and CBM occurs in $[ZnSe_4]^{4-}$ and $[BaSe_7]$ polyhedra and, hence, is a major contribution to the optical activities of Ba_2ZnSe_3. The relationship between the electrode potential for CBM, VBM (EPc, EPv) and Eg can be expressed by the following expressions [62]:

EPc (V vs. NHE) = 1.23–Eg (eV)/2 (1)

EPv (V vs. NHE) = 1.23 + Eg (eV)/2 (2)

The estimated optical band gap of chalcogenide Ba_2ZnSe_3 is 2.70 eV; thus the EPc and EPv are about −0.145 V(vs. NHE) and +2.605 V (vs. NHE), respectively.

To attain solar degradation of pollutants, the reduction capacity of e^- must be able to produce superoxide acid ($-HO_2$) and superoxide anion radicals ($-O^{2-}$), while oxidation of the photogenerated holes (h^+) must be able to oxidize OH^- to produce reactive hydroxyl radicals ($-OH$) [63]. The CBM for photocatalyst material should increase to the vacuum level (EPc will be lower than $H_2 + H/–HO_2$ (vs. NHE) = −0.13 V). Simultaneously, the VBM should rise to a narrow energy band gap and maintain oxidation capacity for h^+ (EPv lower than O_2/H_2O (vs. NHE = +1.23 V)). It is well known that $-OH$ and $-O^{2-}$ are free radicals with high oxidation; thus, $-OH$ and $-O^{2-}$ can oxidize

various organic and inorganic carbon compounds to produce dioxide, water and other non-toxic small organic molecules. Hence, the energy band gap of the photocatalyst determines the range of the solar spectrum absorbed. The narrower the energy band gap, the wider the spectral range response to solar radiation and the more efficiently it can make use of visible light. The location of the CBM and VBM should meet the redox capacity.

Furthermore, the width of the optical band gap is a very important factor for the photocatalyst; in other words, the range of light absorbed (see Fig. 3a,b). The optical absorption induces the transfer of e^- from the VB → CB, generating the $e^- - h^+$ pairs which can then migrate to the surface to participate in oxidation and reduction reactions, respectively [64,65]. Usually the locations of the VBM and the CBM determine the oxidation and reduction capabilities of photogenerated holes and electrons, respectively [64]; the reduction potential level of the electron-acceptors should be energetically below the CBM, whereas the oxidization potential level of the electron-donors should be above the VBM [66]. The optical band gap value of the semiconductor materials can be estimated from the absorption spectrum, as shown in Fig. 3a. From the absorption spectrum, the optical band gap value of the semiconductor can be solved as follows: the square of the absorption coefficient $gI(\omega)$ is linear with photon energy for direct optical transitions in the absorption edge region, whereas the square root of $I(\omega)$ is linear with photon energy for indirect optical transitions [50]. The data plots of $[I(\omega)]^2$ versus photon energy in the absorption edge region are shown in the inset of Fig. 3b. It is clearly shown that $[I(\omega)]^2$ vs photon energy is linear in the absorption edge region. This plot suggests that the absorption edge of the investigated material is caused by direct transitions. Following Fig. 3b, one can conclude that the absorption edge of the investigated material occurs at $\lambda = 459.1$ nm, and the optical band gap is estimated ($\lambda_g = 1239.8/E_{g(optical)}$ [67]) to be 2.70 eV

for chalcogenide Ba_2ZnSe_3.

### 3.2. Photoelectrochemical properties

It has been reported that the mobility of the electrons generated in the photocatalysts can be directly monitored by the generated photocurrent, and the generation rate should directly correlate with the photosensitivity of the material which is used as a photocatalyst [68]. A large generated photocurrent usually signifies a high separation efficiency of e^- and h^+ pairs [52]. For an efficient photocatalytic mechanism, a material with high mobility carriers is required. To achieve this, a material with small effective masses is needed. It was noticed from the electronic band structure of chalcogenide Ba_2ZnSe_3 (Fig. 2a) that the band around the Fermi level (E_F) possesses high k- dispersion bands, which implies low effective masses and, hence, high mobility carriers ($m_e^*/m_o = 0.01271$, $m_{hh}^*/m_o = 0.03022$ and $m_{lh}^*/m_o = 0.01352$), which enhances the charge transfer process; the effective mass provides essential information to reveal the photocatalytic mechanism. The mobility of the photogenerated carriers significantly influences the photocatalytic efficiency [69,70] and higher photogenerated carrier mobility enhances the photocatalytic performance [71]. Moreover, the great effective mass difference ($D = m_e^*/m_{hh}^* = 0.42058$, $D = m_{hh}^*/m_e^* = 2.37766$, $D = m_e^*/m_{lh}^* = 0.94008$ and $D = m_{lh}^*/m_e^* = 1.06373$) between electron and hole can facilitate the electron and hole migration and separation, and finally, improve the photocatalytic performance. The effective mass of an electron is bigger than that of a hole, resulting in a significant difference in the mobility between electron and hole. The mobility of photoexcited carriers can be indirectly assessed by their effective mass ($(mobility)_e = e\tau_e/m_e^*$ and $(mobility)_h = e\tau_h/m_h^*$). A large mobility difference is useful to the separation of e^- and h^+, and the reduction of the

(a) **(b)**
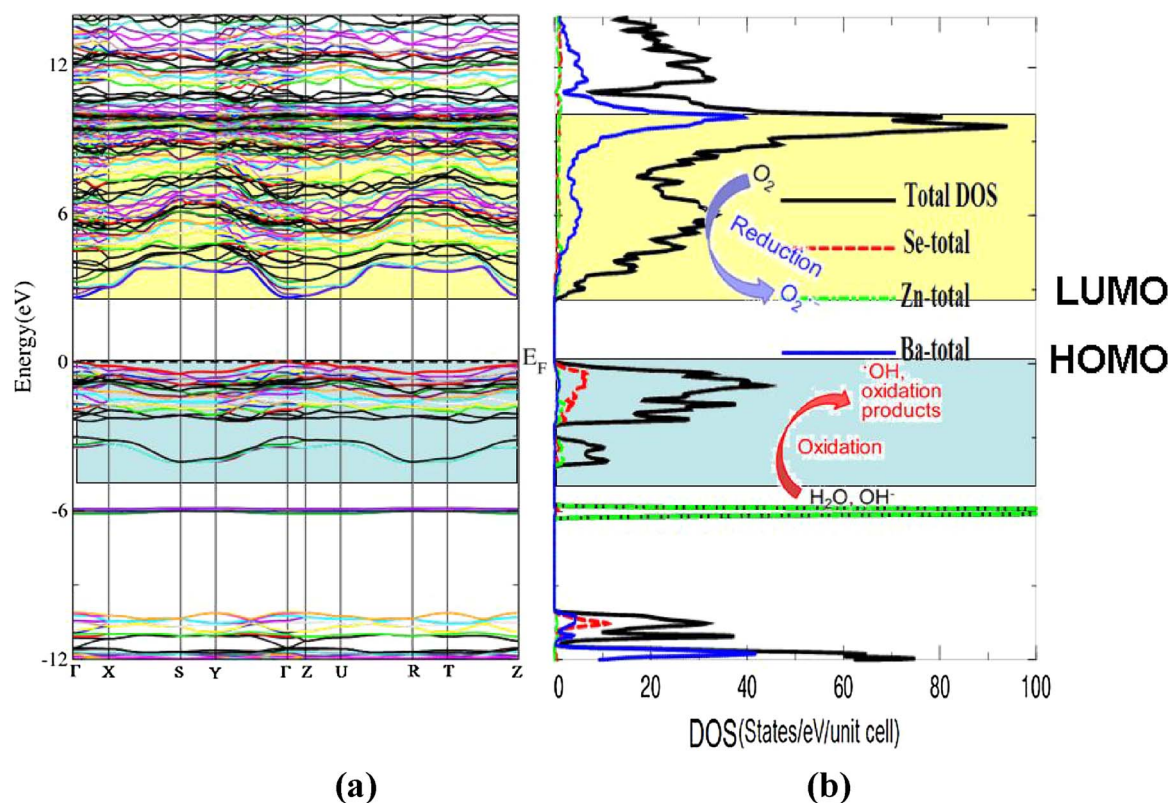
Fig. 2. (a) The calculated electronic band structure of Ba_2ZnSe_3, along with the calculated total density of states; (b) The schematic diagram of charge transfer and the photocatalytic mechanism of Ba_2ZnSe_3. The reactive species induced by illumination are responsible for the photodegradation process. If the energy of the incident photons is larger than the energy band gap of a photocatalyst, the e^- will be excited and transfer to the CBs, leaving h^+ in the VBs. Then the e^- have a great possibility to react with adsorbed oxygen to form another reactive species (superoxide $\cdot O_2^-$). In the meantime, the h^+ can also react with OH^- to generate hydroxyl ($\cdot OH$). The above-generated active species can all participate in the photocatalytic process; **(c-f)** The calculated partial density of states.
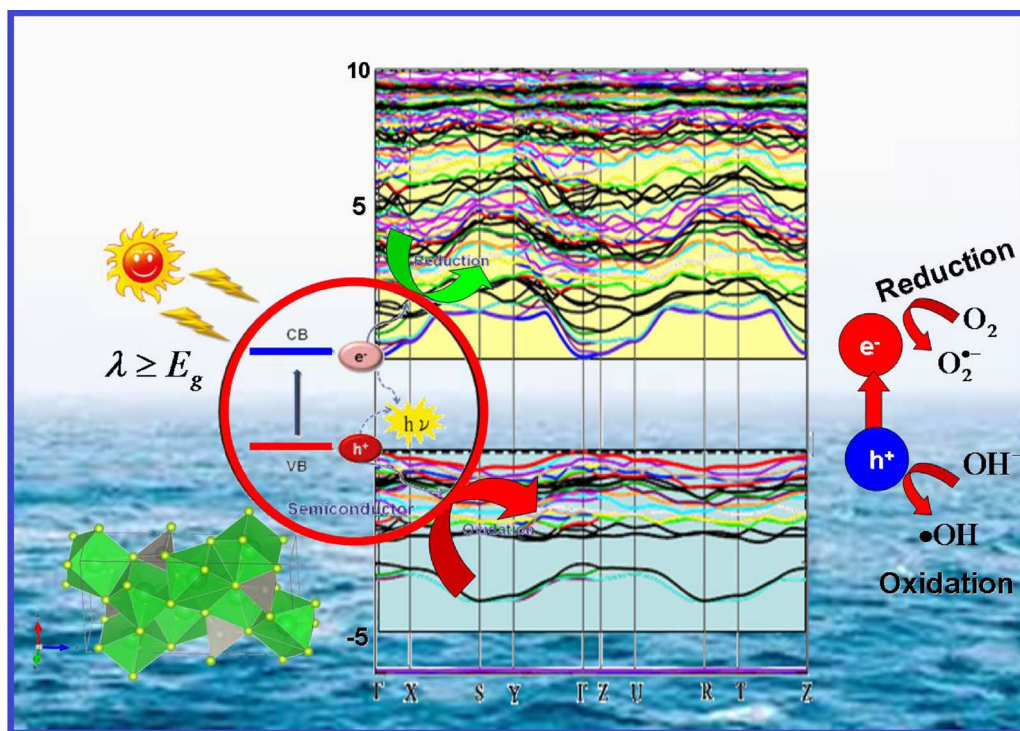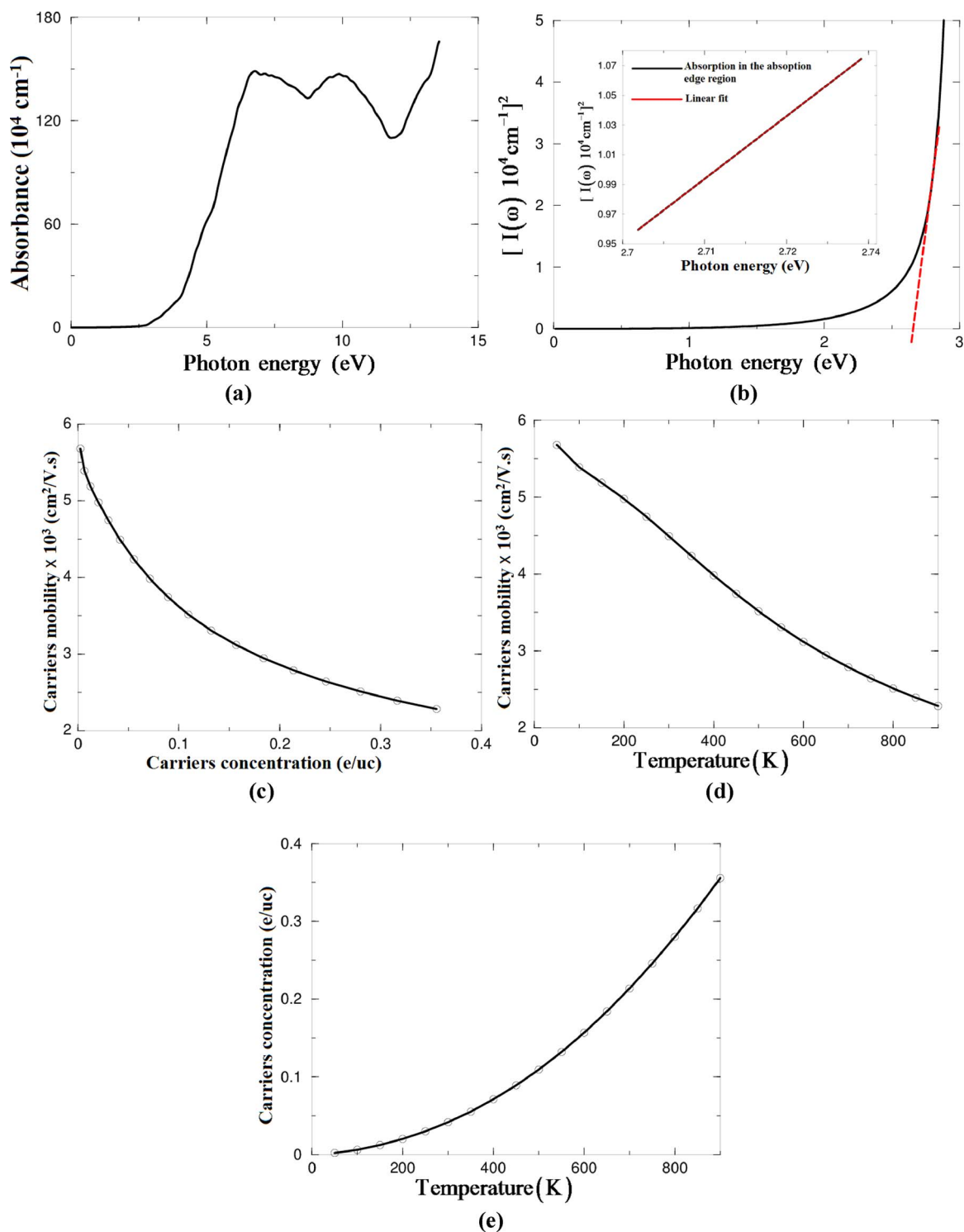
(c)
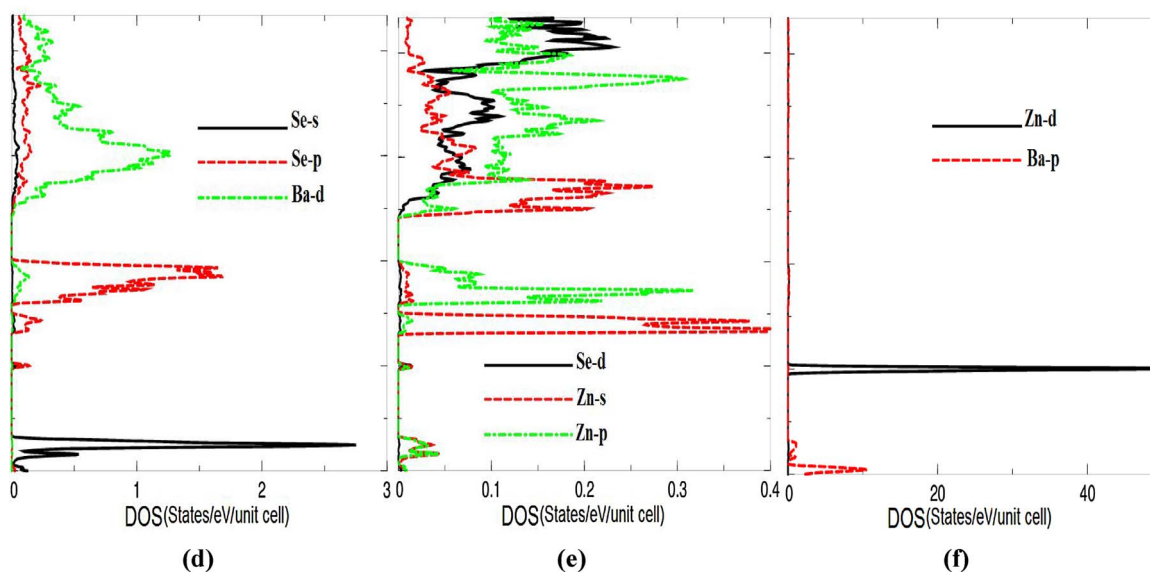
(d)   **(e)**   **(f)**

Fig. 2. (*continued*)

e^- and h^+ recombination rate, and improves the photocatalytic activity. It is clear that the effective mass of the e^- and h^+ are small, and thus, we can deduce that the photogenerated carrier transfer can be fast along different directions. Fig. 3c shows the carriers mobility as a function of carrier concentration (*n*), which clearly shows a significant reduction in the carriers mobility with *n* due to increasing the scattering. To support this statement, we have investigated the carriers mobility as a function of temperature (*T*), as shown in Fig. 3d. It clearly shows a significant reduction in the carriers mobility with an increase in *T*, which is attributed to the fact that raising *T* causes the vibration to increase, and hence, the mobility, resulting in an increase in the scattering which leads to suppression of the mobility.

The other crucial issue to understand the photocatalytic mechanism in chalcogenide Ba_2ZnSe_3 is the carriers concentration (*n*) and their

mobility. Therefore, we have investigated the influence of *T* on the carriers concentration of the chalcogenide Ba_2ZnSe_3 at a certain value of the chemical ($\mu = E_F$). It is clear that carriers concentration (Fig. 3e) exponentially increases with increasing *T*. To support this statement, we have *n* as a function of chemical potential in the vicinity of E_F at three *T* values, as shown in Fig. 3f. It was noticed that the difference between chemical potential and Fermi energy ($\mu - E_F$) is positive for VBs and negative for CBs, and the chalcogenide Ba_2ZnSe_3 exhibits a maximal *n* in the vicinity of E_F. Furthermore, the photoconductivity as a function of photon energy was investigated, as shown in Fig. 3g. It is clear that the chalcogenide Ba_2ZnSe_3 shows the highest photoconductivity when the photons possess an energy of about 2.70 eV. Thus, it covers the visible region. Apparently, the photocurrent is generated immediately at the absorption edge, i.e. 2.70 eV, which implies that the

Fig. 3. (a) Calculated absorptance as a function of photon energy; (b) From the absorption spectrum, the optical band gap value of the semiconductor can be solved as follows: the square of the absorption coefficient I(ω) is linear with photon energy for direct optical transitions in the absorption edge region, whereas the square root of I(ω) is linear with photon energy for indirect optical transitions. The data plots of [I(ω)]^2 versus photon energy in the absorption edge region are shown in the inset of Fig. 3b. It is clearly shown that [I(ω)]^2 vs. photon energy is linear in the absorption edge region. This plot suggests that the absorption edge of the investigated material is caused by direct transitions. Following Fig. 3b, one can conclude that the absorption edge of the investigated material occurs at λ = 459.1 nm, and the optical band gap is estimated to be 2.70 eV for chalcogenide Ba$_2$ZnSe$_3$; (c) The mobility of Ba$_2$ZnSe$_3$ as a function of carrier concentration; (d) The mobility of Ba$_2$ZnSe$_3$ as a function of temperature; (e) The carrier concentration of Ba$_2$ZnSe$_3$ as function of temperature; (f) The carrier concentration of Ba$_2$ZnSe$_3$ as a function of chemical potential $\mu - E_F$ at room temperature and two other randomly selected temperatures; (g) The photoconductivity of Ba$_2$ZnSe$_3$ as a function of photon energy.

(f)

(g)

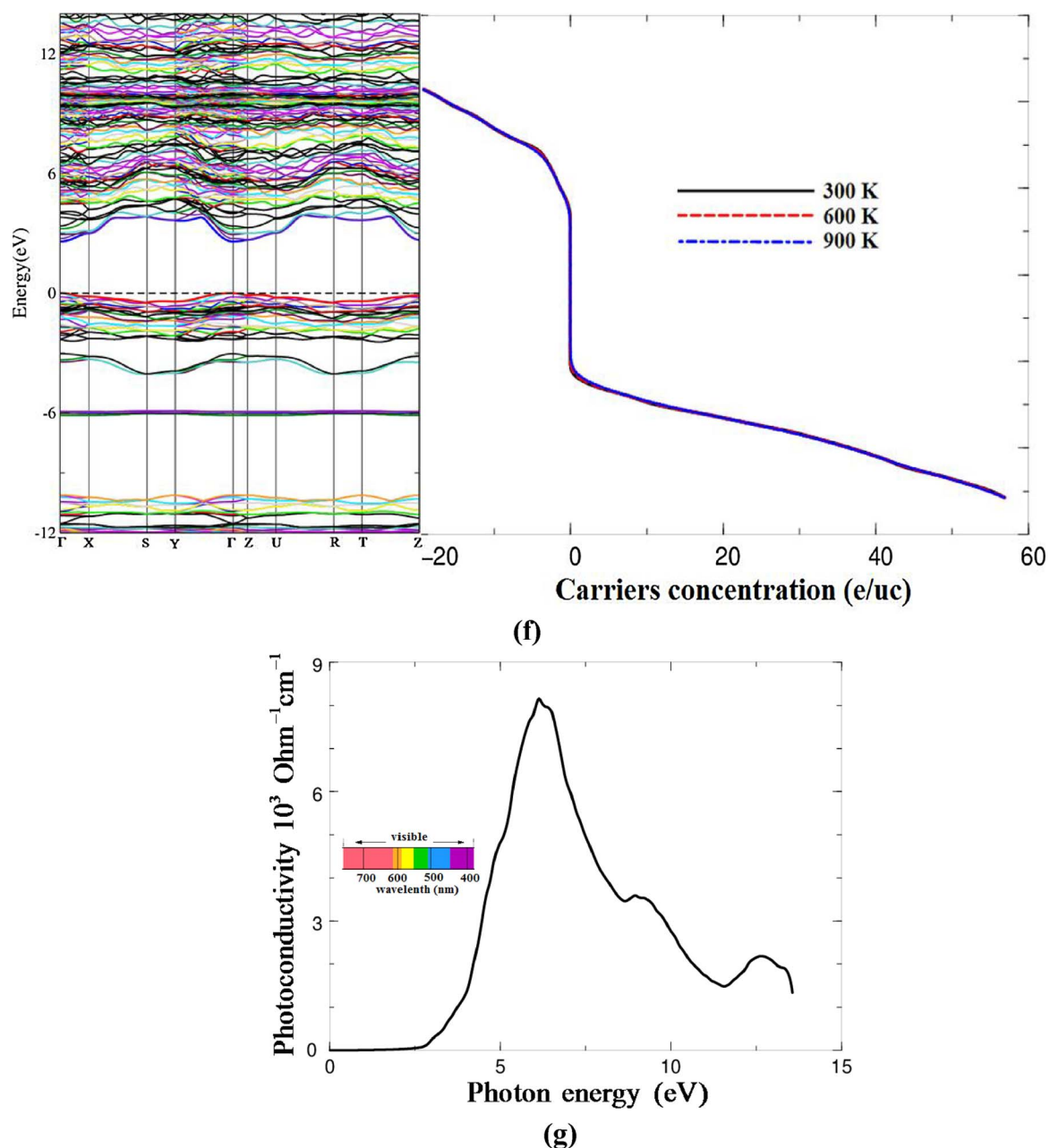**Fig. 3.** (*continued*)

chalcogenide Ba_2ZnSe_3 exhibits photocurrent response in the visible light region. This indicates that the investigated material may have good photocatalytic activity and agrees well with the foregoing photocatalytic activity measurement.

3.3. Electronic charge density

In order to reveal the chemical bonding properties of chalcogenide Ba_2ZnSe_3, the electronic charge density was calculated, as shown in Fig. 4(a–f). The charge localizes mainly between Zn and the neighboring Se, also between Ba and Se atoms, indicating a partial ionic and strong covalent bonding. The strength of the interactions between the atoms is due to the degree of the hybridization and the electronegativity differences. According to the Pauling scale, the electronegativity of Ba, Zn and Se are 0.89, 1.65 and 2.55, respectively. To describe the character of the chemical bonding in chalcogenide Ba_2ZnSe_3, the difference of the electronegativity $(X_A - X_B)$ is crucial [54], where X_A and X_B denote the electronegativity of the A and B atoms in general. With an increase in the $(X_A - X_B)$ difference, the ionic character (P) of the bonding increases. The percentage of P for the chemical bonding can be obtained using the expression [72]:

$$P(\%) = 16(X_A - X_B) + 3.5(X_A - X_B)^2 \qquad (3)$$

The calculated values of P are given in Table 1. It is clear that the $Zn-Se$ bonds in the $ZnSe_4$ units and the $Ba-Se$ bonds in $BaSe_7$ units are mostly covalent and partially ionic bonding. The covalent bonding is more favorable for the transport of the carriers than ionic bonding [73]. Also, due to the electronegativity differences between the atoms, some valence electrons are transferred to Se atoms, as it is clear that these atoms are surrounded by uniform blue spheres, which indicate the maximum charge accumulation according to the thermoscale (Fig. 4g). The $Zn-Se$ and $Ba-Se$ bonds possess strong electron cloud overlap and prefer to attract holes and repel electrons, thus facilitating separation of the photogenerated $e^- - h^+$ pairs. This in turn enhances the photocatalytic activity [74].

4. Conclusion

The excellent photocatalytic performance in Ba_2ZnSe_3 is due to hyperpolarizability formed by ZnO_4 tetrahedra and co-parallel $BaSe_7$ polyhedra groups. The newly discovered Ba_2ZnSe_3 crystal almost doubles the efficiency of the photocatalytic performance of chalcogenide crystals due to the presence of the distorted $(ZnO_4)^{4-}$ tetrahedral. Moreover, the introduction of Zn atoms causes blue-shift of the Ba_2ZnSe_3 absorption edge to 459.1 nm. We investigated the influence of $(ZnO_4)^{4-}$ tetrahedra and co-parallel $BaSe_7$ polyhedra groups on the crystal structure, and hence, on the resulting photocatalytic performance. Our investigation confirms that Ba_2ZnSe_3 possesses large birefringence, has considerable anisotropy in the optical response, and the absorption edge occurs in the visible region. Therefore, based on these promising results, we calculated photocatalytic performance in Ba_2ZnSe_3 and found that the distorted $(ZnO_4)^{4-}$ tetrahedra are the main source of the increase in the efficiency of the photocatalytic performance. The crystal structure consists of layers; the $ZnSe_4$ groups originate from the connection of one Zn with four Se, while $BaSe_7$ originates from the connection of one Ba with seven Se. The layers structure favors the enhancement of the photocatalytic performance.

The estimated optical band gap of Ba_2ZnSe_3 is 2.70 eV, and the EPc and EPv are about − 0.145 V(vs. NHE) and + 2.605 V (vs. NHE), respectively. Thus, Ba_2ZnSe_3 possesses a high negative reduction potential of excited electrons due to its higher CB position, and hence, the location of the CBM and VBM accommodates the redox capacity. As a result, the Ba_2ZnSe_3 photocatalyst is expected to exhibit superior activity in visible-light-driven photocatalytic H_2 evolution. The electronic band structure shows high k-dispersion bands around E_F, which implies low effective masses and, hence, the high mobility carriers enhance the charge transfer process. It was found that Ba_2ZnSe_3 possesses a great effective mass difference between e^- and h^+, which can facilitate the e^- and h^+ migration and separation, and finally, improve the photocatalytic performance. The observed large mobility difference in Ba_2ZnSe_3 is useful to the separation of e^- and h^+, reduction of the e^- and h^+ recombination rate, and improvement of the photocatalytic activity. Therefore, Ba_2ZnSe_3 could be a good photocatalyst due to rapid generation of $e^- – h^+$ pairs with photoexcitation, and a high negative reduction potential of excited electrons due to its higher CB position. Based on these results, one can conclude that Ba_2ZnSe_3 satisfies all requirements to be an efficient photocatalyst. This will greatly improve the search efficiency and greatly help experiments to save
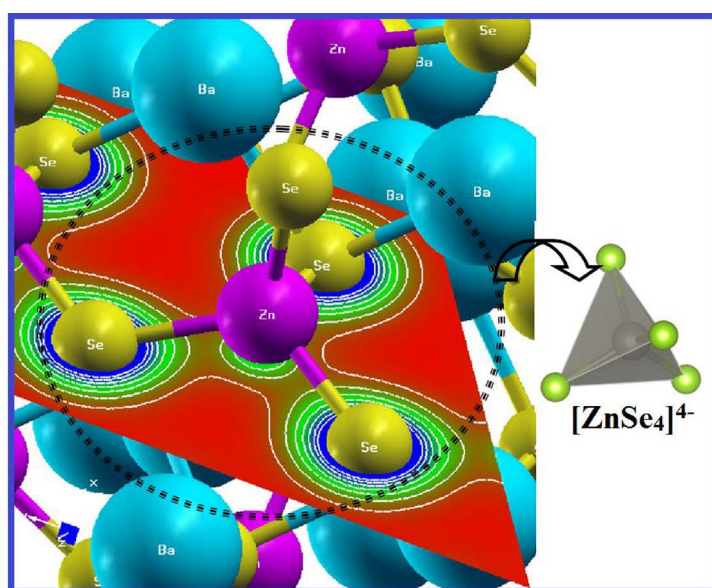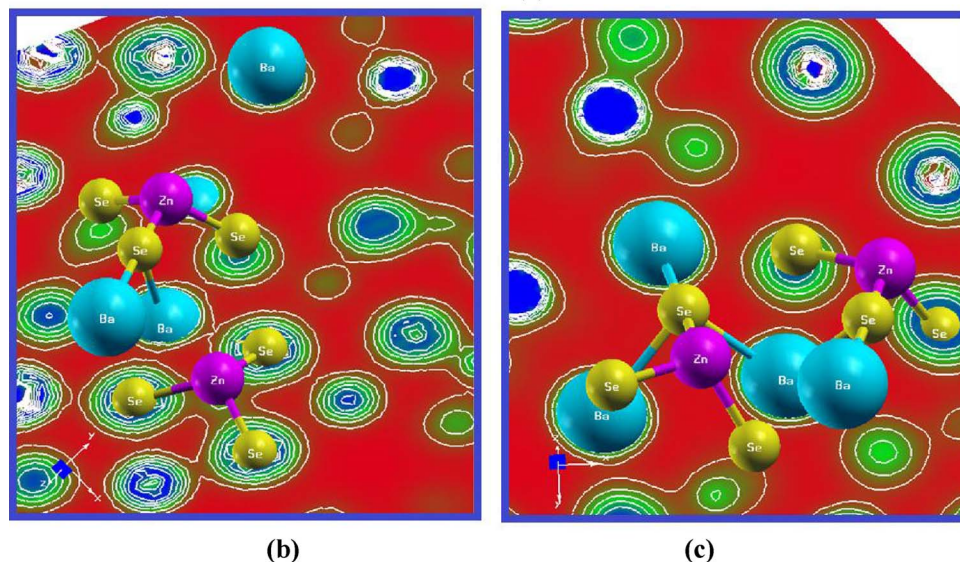

(a)

Fig. 4. (a-f) Calculated electronic charge density distribution which shows that Zn−Se and Ba−Se bonds possess strong electron cloud overlap and prefer to attract holes and repel electrons, thus facilitating separation of the photogenerated $e−h$ pairs. This in turn enhances the photocatalytic activity; **(g)** Thermoscale.
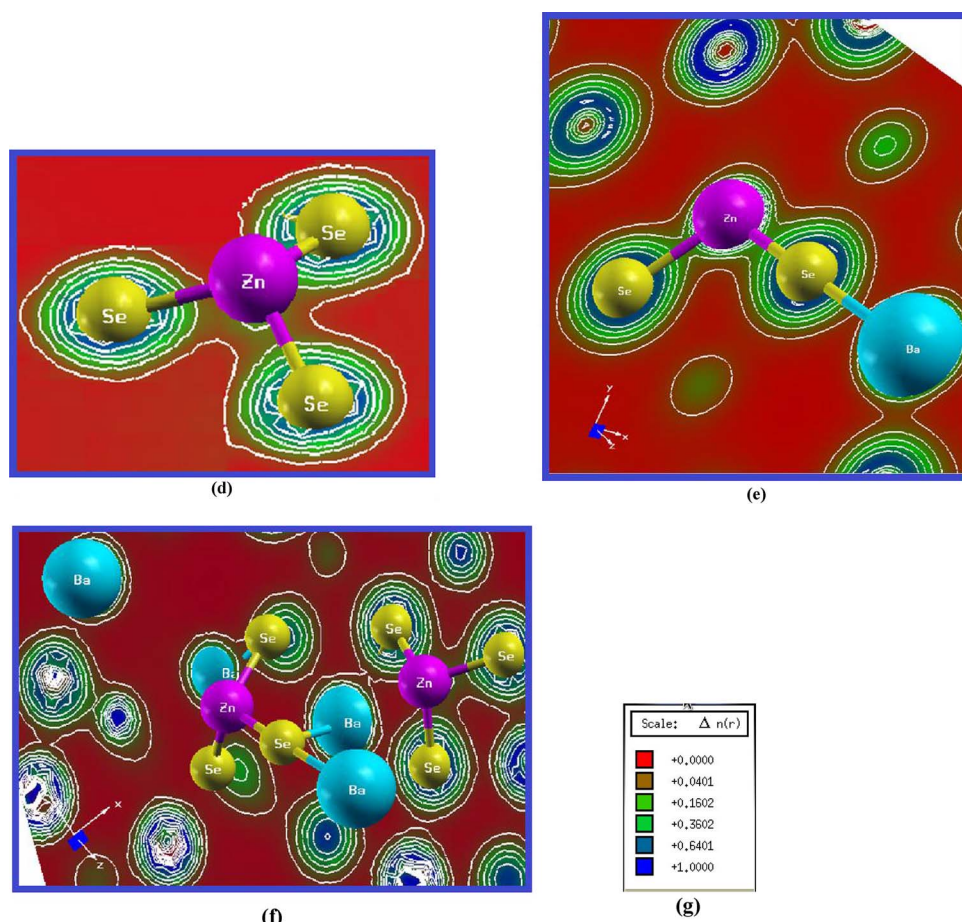

(b)

(c)

Fig. 4. (*continued*)

(d)

(e)

(f)

(g)

resources in the exploration of new photocatalysts with good photocatalytic performance.

Author contribution

A. H. Reshak, as a professor with PhD in physics and PhD in materials engineering has performed the calculations, analyzing and discussing the results and writing the manuscript.

Competing financial interests

The author declare no competing financial interests.

Acknowledgments

Table 1
The calculated values of the ionic character.

Bonds	P(%)
Zn-Se	17.23
Ba-Se	36.20

Appendix A. Supplementary data

Supplementary data associated with this article can be found, in the online version, at http://dx.doi.org/10.1016/j.apcatb.2017.09.018.

References

[1] M. Muruganandham, R. Amutha, G.J. Lee, S.H. Hsieh, J.J. Wu, M. Sillanpää, J. Phys. Chem. C 116 (2012) 12906–12915.
[2] L. Huang, X.L. Wang, J.H. Yang, G. Liu, J.F. Han, C. Li, J. Phys. Chem. C 117 (2013) 11584–11591.
[3] T. Wen, D.X. Zhang, J. Zhang, Inorg. Chem. 52 (2013) 12–14.
[4] X. Fan, L. Zang, M. Zhang, H. Qiu, Z. Wang, J. Yin, H. Jia, S. Pan, C. Wang, Chem. Mater. 26 (2014) 3169–3174.
[5] H. Tong, S.X. Ouyang, Y.P. Bi, N. Umezawa, M. Oshikiri, J.H. Ye, Adv. Mater. 24 (2012) 229–251.
[6] Z. Li, X. Chen, W. Shangguan, Y. Su, Y. Liu, X. Dong, P. Sharma, Y. Zhang, Int. J. Hydrogen Energy 42 (2017) 6618–6626.
[7] S. Khan, M. Al-Shahry, W.B. Ingler, Science 297 (2002) 2243–2244.
[8] A. Kudo, Y. Miseki, Chem. Soc. Rev. 38 (2009) 253e78.
[9] X.B. Chen, S.H. Shen, L.J. Guo, S.S. Mao, Chem. Rev. 110 (2010) 6503–6570.
[10] H.B. Yi, T.Y. Peng, D.N. Ke, D. Ke, L. Zan, C.H. Yan, Int. J. Hydrogen Energy 33 (2008) 672–678.
[11] C.C. Hu, H. Teng, J. Catal. 272 (2010) 1–8.
[12] K.E. Dekrafft, C. Wang, W.B. Lin, Adv. Mater. 24 (2012) 2014–2018.
[13] C. Xu, Y. Zhang, J. Chen, J. Lin, X. Zhang, Z. Wang, J. Zhou, Appl. Catal. B-Environ. 204 (2017) 324–334.
[14] L. Sun, W. Zhou, Y. Liu, D. Yu, Y. Liang, P. Wu, Appl. Surf. Sci. 389 (2016) 484–490.
[15] W. Yua, J. Zhang, T. Peng, Appl. Catal. B-Environ. 181 (2016) 220–227.
[16] J. Zhang, P. Zhou, J. Liu, J. Yu, Phys.Chem.Chem.Phys 16 (2014) 20382–20386.
[17] M. Dong, J. Zhang, J. Yu, APL Mater. 3 (2015) 104404.
[18] J. Zhang, S. Wageh, A.A. Al-Ghamdi, J. Yu, Appl. Catal. B-Environ. 192 (2016) 101–107.
[19] Y. Li, C. Cai, Y. Gu, W. Cheng, W. Xiong, C. Zhao, Appl. Surf. Sci. 414 (2017) 34–40.
[20] S. Na Phattalung, S. Limpijumnong, J. Yu, Appl. Catal. B-Environ. 200 (2017) 1–9.
[21] Qing Han, Nan Chen, Jing Zhang, Liangti Qu, Mater. Horiz. (2017), http://dx.doi.org/10.1039/C7MH00379J.

[22] Deqian Zeng, Wee-Jun Ong, Hongfei Zheng, Mingda Wu, Yuanzhi Chen, Dong-Liang Peng, Ming-Yong Han, J. Mater. Chem. A (2017), http://dx.doi.org/10.1039/C7TA04816E.
[23] W.-J. Ong, L.K. Putri, Y.-C. Tan, L.-L. Tan, N. Li, Y.H. Ng, X. Wen, S.-P. Chai, Nano Res. 10 (2017) 1673–1696.
[24] Q. Han, B. Wang, J. Gao, Z. Cheng, Y. Zhao, Z. Zhang, L. Qu, ACS Nano 10 (2016) 2745–2751.
[25] Q. Han, B. Wang, J. Gao, L. Qu, Angew. Chem. Int. Ed. 55 (2016) 10849–10853.
[26] W.-J. Ong, L.K. Putri, L.-L. Tan, S.-P. Chai, S.-T. Yong, Appl. Catal. B-Environ. 180 (2016) 530–543.
[27] N.Z. Bao, L.M. Shen, T. Takata, K. Domen, Chem. Mater. 20 (2008) 110–117.
[28] M. Matsumura, S. Furukawa, Y. Saho, H. Tsubomura, J. Phys. Chem. 89 (1985) 1327–1329.
[29] S.W. Liu, J.G. Yu, M. Jaroniec, J. Am. Chem. Soc. 132 (2010) 11914–11916.
[30] J.R. Ran, J.G. Yu, M. Jaroniec, Green Chem. 13 (2011) 2708–2713.
[31] H.L. Wang, L.S. Zhang, Z.G. Chen, J.Q. Hu, S.J. Li, Z.H. Wang, J.S. Liu, X.C. Wang, Chem. Soc. Rev. 43 (2014) 5234–5244.
[32] R. Asahi, T. Morikawa, T. Ohwaki, K. Aoki, Y. Taga, Science 293 (2001) 269–271.
[33] H. Li, J. Shang, Z.H. Ai, L.Z. Zhang, J. Am. Chem. Soc. 137 (2015) 6393–6399.
[34] S. Khanchandani, S. Kumar, A.K. Ganguli, ACS Sustain. Chem. Eng. 4 (2016) 1487–1499.
[35] U. Soni, P. Tripathy, S. Sapra, J. Phys. Chem. Lett. 5 (2014) 1909–1916.
[36] M.D. Regulacio, M.Y. Han, Acc. Chem. Res. 49 (2016) 511–519.
[37] S.L. Xiong, B.J. Xi, C.M. Wang, G.C. Xi, X.Y. Liu, Y.T. Qian, Chem. − Eur. J. 13 (2007) 7926–7932.
[38] M.J. Tafreshi, K. Balakrishnan, R. Dhanasekaran, J. Mater. Sci. 32 (1997) 3517–3521.
[39] Y.D. Li, Y. Ding, Y.T. Qian, Y. Zhang, L. Yang, Inorg. Chem. 37 (1998) 2844–2845.
[40] A.B. Panda, G. Glaspell, M.S. El-Shall, J. Am. Chem. Soc. 128 (2006) 2790–2791.
[41] Y.C. Zhu, Y. Bando, Chem. Phys. Lett. 377 (2003) 367–370.
[42] J.Q. Hu, Y. Bando, J.H. Zhan, Z.W. Liu, D. Golberg, S.P. Ringer, Adv. Mater. 17 (2005) 975–979.
[43] L.H. Zhang, H.Q. Yang, J. Yu, F.H. Shao, L. Li, F.H. Zhang, H.J. Zhao, Phys. Chem. C 113 (2009) 5434–5443.
[44] M. Zhou, K. Xiao, X. Jiang, H. Huang, Z. Lin, J. Yao, Y. Wu, Inorg. Chem. 55 (2016) 12783–12790.
[45] J. Prakash, A. Mesbah, J. Beard, D. Rocca, S. Lebègue, C.D. Malliakas, J.A. Ibers, Z. Naturforsch. 71 (2016) 425–429.
[46] J.P. Perdew, S. Burke, M. Ernzerhof, Phys. Rev. Lett. 77 (1996) 3865.
[47] P. Blaha, K. Schwarz, G.K.H. Madsen, D. Kvasnicka, J. Luitz, WIEN2k, An Augmented Plane Wave Plus Local Orbitals Program for Calculating Crystal Properties, Vienna University of Technology, Austria, 2001.
[48] F. Tran, P. Blaha Phys. Rev. Lett. 102 (2009) 226401.
[49] V.V. Atuchin, T.A. Gavrilova, J.-C. Grivel, V.G. Kesler, Surf. Sci. 602 (2008) 3095–3099;

V.V. Atuchin, T.A. Gavrilova, J.-C. Grivel, V.G. Kesler, J. Phys. D: Appl. Phys. 42 (2009) 035305;
O.Y. Khyzhun, V.L. Bekenev, V.V. Atuchin, E.N. Galashov, V.N. Shlegel, Mater. Chem. Phys. 140 (2013) 558–595;
V.V. Atuchin, E.N. Galashov, O.Y. Khyzhun, V.L. Bekenev, L.D. Pokrovsky, V.N. Borovlev, J, Solid State Chem. 236 (2016) 3–24.
[50] H. Huang, Xu Han, X. Li, S. Wang, P.K. Chu, Y. Zhang, ACS Appl. Mater. Interfaces 7 (2015) 482–492;
H. Huang, X. Li, J. Wang, F. Dong, P.K. Chu, T. Zhang, Y. Zhang, ACS Catal. 5 (2015) 4094–4103.
[51] H. Huang, Y. He, X. Li, M. Li, C. Zeng, F. Dong, X. Du, T. Zhangd, Y. Zhang, J. Mater. Chem. A 3 (2015) 24547–24556.
[52] H. Huang, Y. He, Z. Lin, L. Kang, Y. Zhang, J. Phys. Chem. C 117 (2013) 22986–22994.
[53] J. Zhang, W. Yu, J. Liu, B. Liud, Appl. Surf. Sci. 358 (2015) 457–462.
[54] X. Li, J. Zhao, J. Yang, Sci. Rep. 3 (2013) 1858.
[55] D.W. Hwang, J.S. Lee, W. Li, S.H. Oh, J. Phys. Chem. B 107 (2003) 4963–4970.
[56] C. Liu, Y. Zhang, F. Dong, A.H. Reshak, L. Ye, N. Pinna, C. Zeng, T. Zhang, H. Huang, Appl. Catal. B-Environ. 203 (2017) 465–474.
[57] A.H. Reshak, J. Catal. 352 (2017) 142–154.
[58] A.H. Reshak, J. Catal. 351 (2017) 119–129.
[59] A.H. Reshak, S. Auluck, J. Catal. 351 (2017) 1–9.
[60] H. Huang, S. Tu, C. Zeng, T. Zhang, A.H. Reshak, Y. Zhang, Angew. Chem. Int. Ed. (2017), http://dx.doi.org/10.1002/anie.201706549.
[61] P. Zhou, J.H. Wu, W.L. Yu, G.H. Zhao, G.J. Fang, S.W. Cao, Appl. Surf. Sci. 319 (2014) 167–172.
[62] Y. Matsumoto, J. Solid State Chem. 126 (1996) 227–234.
[63] D. Dvoranová, V. Brezová, M. Mazúra, M.A. Malati, Appl. Catal. B-Environ. 37 (2002) 91–105.
[64] J. Zhang, W. Yu, J. Liu, B. Liu, Appl. Surf. Sci. 358 (2015) 457–462.
[65] J.C. Wu, J.W. Zheng, P. Wu, R. Xu, J. Phys. Chem. C 115 (2011) 5675–5682.
[66] S. Banerjee, J. Gopal, P. Muraleedharan, A.K. Tyagi, B. Raj, Curr. Sci. 90 (2006) 1378–1383.
[67] J.M. Carlsson, B. Hellsing, H.S. Domingos, P.D. Bristowe, Phys. Rev. B 65 (2002) 205122–205132.
[68] H.G. Kim, P.H. Borse, W.Y. Choi, J.S. Lee, Angew. Chem. Int. Ed. 44 (2005) 4585–4589.
[69] J.W. Tang, J.H. Ye, Chem. Phys. Lett. 410 (2005) 104–107.
[70] T.L. Bahers, M.R. rat, P. Sautet, J. Phys. Chem. C 118 (2014) 5997–6008.
[71] J. Sato, H. Kobayashi, Y. Inoue, J. Phys. Chem. B 107 (2003) 7970–7975.
[72] Schlusseltechnologien Key Technologies, Vol. 11, ISBN 978-3-89336-559-3, 41 st IFF Spring school, 2010, pp A1–18.
[73] F. Wu, H.Z. Song, J.F. Jia, X. Hu, Prog. Nat. Sci.: Mater. Int. 23 (2013) 408–412.
[74] X. Fan, L. Zang, M. Zhang, H. Qiu, Z. Wang, J. Yin, H. Jia, S. Pan, C. Wang, Chem. Mater. 26 (2014) 3169–3174.